Simulation of Thermal Spray Coating on 3D Objects: Numerical Scheme and Aeronautic Test Case

T. Van Hoof[1] · G. Fradet[2] · F. Pichot[2] · S. Selezneff[2] ·
N. Poletz[1]

Abstract A novel numerical methodology is proposed to simulate thermal spray coating process on 3D objects with a focus on the prediction of the footprint shape and thickness. The method is based on the level set approach to capture the evolution of the deposited layer interface during the coating process. The shadowing effects that strongly affect the final footprint on 3D objects are considered. The method allows for the imposition of complex source trajectory and orientation evolution which are requested to tailor the final footprint on complex 3D objects. The capabilities and limitations of the proposed numerical tools are assessed using an aeronautic test case: the thermal spray coating of a part of aircraft engine (seal teeth).

Introduction

The thermal spraying industry has been rising since the 1960s with the aerospace industry as a major contributor (Ref 1). The applications are mainly for aircraft engines, where it is possible to find a large number of parts coated with a wide variety of properties (anti-fretting, anti-erosion, thermal barrier, abradable, etc.) (Ref 2).

✉ T. Van Hoof
thibaut.vanhoof@cenaero.be

1 Cenaero, 29, Rue des Frères Wright, 6041 Gosselies, Belgium

2 Safran Aircraft Engines, rue Henri Auguste Desbruères, 91003 Evry, France

Thermal spray processes are divided into two main categories (Ref 3). Among the most common used is the spraying by atmospheric plasma (APS), as this is known as the most flexible and it can be used to melt and spray a large range of materials such as polymers, metals and ceramics. The plasma flame is obtained by ionizing of gas mixture (Ar, H_2, N_2, He) from electric discharge between anode and cathode. The powder particles are injected through the flame, heated and accelerated toward the substrate. So, a coating is formed in a chaotic manner with the stacking of (partially) melted particles also commonly called as splats (Ref 3). Thermal spraying is a surface coating process involving more than thirty variables (powder morphology, particle injection rate, plasma gas composition, etc.). The final properties of coating are strongly governed by the deposition process parameters.

The main innovation perspectives focus on (i) new coatings with understanding of the physical phenomena involved (flame/powder interactions, etc.), (ii) optimization of continuous controls (robot movement, etc.) and (iii) non-destructive testing of coatings properties (Ref 1). The aeronautical industry must constantly increase its production rates and therefore the industrialization of parts. For thermal spray, this involves the design of several tools and the creation of many robot / guns kinematic. Many parts are sacrificed to ensure the compliance of the coating with technical requirements. This requires an iterative approach of trials and errors, especially on complex parts as sealing teeth. To limit these industrialization costs, numerical simulation of the coating thickness on the substrate is an important technology which allows reducing the number of experimental iterations.

The objective of the present work is to develop a numerical tool able to predict the shape and thickness of the coating layer (footprint) for a thermal spray coating process on

a complex 3D object. The goal of this tool is to assist the definition of the experimental coating procedure for a given complex 3D object through fast and reliable predictions of the influence of process parameters, mainly the source characteristics and trajectory, on the final coating footprint.

The paper is organized as follows: a review of the state of the art, regarding the numerical simulation of thermal spray process is performed in section "State of the Art". In section "Experimental Procedure", the experimental procedures for the characterization of the deposition rate profile and the industrial test case are described. The proposed numerical model is described in section "Numerical Method". Section "Model Assessment" is devoted to the analysis of the numerical results and the assessment of the model through comparison of the predicted footprint with the experimental measurements for the selected industrial test case.

State of the Art

Regarding the complex component's geometries to coat that can be faced in aerospace industry, the interest in developing numerical simulation models has become greater. Thus, predicting the coating thickness related with the process parameters such as spray angle, combined motion between part and spray gun could bring useful information to set up the process. Further applications could also consist in taking into account the process effect on the component material. For example, by simulating the thermal field induced during the process and the subsequent metallurgical modifications that can occur (residual stress). Therefore, and following the aimed goal, the whole process of thermal spray could be approached in several manners.

Data Analysis

Cirolini and al. (Ref 4) used a set of physical rules to feed a parameter analysis, taking into account process parameters such as plasma temperature, particles size and distribution to first determine the coating profile and then the thermal stresses (Ref 4). Some other authors performed data analyses to build links between the process parameters spray distance, spray angle, angular positioning of the powder injection and the morphologies of the coating thickness. Following this approach, Trifa and al. (Ref 5) found that the spray angle is one of the main contributors to coat morphology (coat height, asymmetry).

Plasma Spray Computation

To better understand the complex phenomena occurring and to investigate from a physical point of view, the interaction between process parameters (spraying angle, distance, carrier gas flow, electrical power…) and particles speeds, trajectories, temperatures and several studies have been carried out (Ref 6). Ko and al. (Ref 7) developed a Computational Fluid Dynamics model in order to investigate the effect of the velocity ratio of carrier gas and plasma jet, particle injection position, particle size, particle density on particle deposition velocity, geometrical uniformity of the coating and particle deposition performance. The results obtained showed that obviously, the velocity ratio has a significant impact on the three indicators and reaches an optimum for a 1/100 value. On the other hand, the carrier gas injection position directly influences on the uniformity of the coating. Finally, it was shown that the smaller the particle distribution, the best the deposition performance is. Gawne et al. (Ref 8) also investigated the links between the gas flow and the powder particles. Instead of using a conventional individual-oriented particle model monitoring velocity and temperature of each particle, the authors used parcels of particles and also used a normal particle size distribution instead of an average diameter. The results indicate that the gas–particle interaction produces irregularities in the pattern of the plasma jet. This phenomenon is due to the asymmetry given by the lateral injection of the powder in the gas flow and the random components in the injection velocity and the size of the feedstock particles.

Above a critical feed rate, the interactions between particle and gas flow should not be neglected. Gu et al. (Ref 9) tried to figure out the physical coupling between particle and gas taking into account the non-spherical geometry of some powders produced by milling. They showed, by setting up a CFD model, that the non-spherical particles are predicted to stay closer to the center of the gas flow, get more momentum and less heat due to their geometry which make them easier to carry.

Remesh et al. (Ref 10), Kotowski et al. (Ref 11) combined a CFD simulation of the thermal spray modeling with a mathematical model to estimate the profile of the geometry deposited on the substrate. In their study, Remesh et al. found that the powder carrier gas flow rate influences the particle distribution on the substrate by imparting a radial injection momentum, which is greater following the increasing size of the particles and that causes elliptical-shaped particle deposition on the substrate. Kotowski et al. used a software solution called "*Jets&Poudres*" to first be able to track the current position, velocity and the fusion process of powder particles as well as conducting the basic analysis of obtained coating formed during the plasma spraying process. This last type of models is very relevant from an industrial point of view as they are more focused on the resulting coating geometry and the following thermal stresses induced whereas being purely focused on the particle–gas flow interaction.

Coating Footprint Prediction

Due to the lack of powerful calculation machines and tools, by the past several authors focused their approaches by using the available experimental data and semi-analytical models. For example, in the early nineties, Goedjen et al. (Ref 12) set up a finite difference-based model to predict the thickness of coatings deposited using the thermal spray process. They developed a two-dimension model, which take into account the relative motion between the part and the robot automaton and evaluate the influence on the coating thickness for a spraying on a simple disk geometry. The matter feed is directly linked to a Gaussian repartition, which is integrated to get related to the coating dimensions. Thereby, the coating thickness on one point is described by the following equation:

$$\mathrm{d}T = R \cdot \mathrm{d}t \tag{1}$$

where $\mathrm{d}T$(m) is the deposit thickness increment, R(m/s) is the deposition rate of the thermal-sprayed powder and $\mathrm{d}t$(s) is the time step. The results obtained showed the feasibility to use such model. However, the author emphasizes the need for building a 3D model.

Fasching et al. (Ref 13) proposed a technique to optimize the spray gun trajectory in order to avoid the asymmetrical resulting coating geometries. The asymmetry was characterized by a statistical variable and simulations are performed to evaluate the best torch angle to symmetrize the coating geometry.

Stepanenko proposes to extend the model of Goedjen et al. to account for time-dependent material feed rate (Ref 14). Recently, Fanicchia and Axinte propose a coating model coupled with a thermal model in order to include the effects of surface temperature on the deposition efficiency (the ratio of material deposited on the surface over the total amount of material injected in the plasma source) (Ref 15).

Proposed Numerical Methodology

Most of the existing numerical methodologies deal with the coating of 2D or flat 3D objects (like cylinder). The simulation of the coating of a complex 3D-shaped object remains a challenging target for modeling. The coating thickness depends on the relative orientation between the source and the target surface (Ref 5). In the case of 3D object, the surface orientation is not uniform leading to large variations of the coating thickness on the object. Moreover, the coating of a 3D object involves strong shadowing effects, which also affect the final coating footprint. Depending on the relative orientations between the object and the source, some regions of the object may hide other regions leading to shadows where no deposition occurs.

In order to control the final footprint on 3D object and reach the target distribution of deposited layer thickness, the source and/or the object are moved following complex trajectories. The adjustment of the source/object trajectories is a complex problem, which may benefit from fast numerical models able to predict the impact of trajectory on the final footprint. The numerical model proposed in section "Numerical Method" is a first step toward such fast numerical footprint simulations on complex 3D objects.

The present model focuses on the mass transfer toward the object surface. The complex plasma behaviors and the thermo-fluid interactions between carrier gas and the particles are not explicitly simulated. Also, the thermal and mechanical effects of the coating process on the surfaces are not considered at this stage. However, these phenomena may affect the targeted mass transfer. Indeed, the temperature and roughness of the surface and the particles mass, shape and melting state may affect the deposition efficiency (Ref 15). In the present work, a phenomenological approach is used to approximate these complex phenomena: the material deposition rate distribution used as input of the 3D coating simulation is adjusted to reproduce the footprint obtained with simple 2D coating process (see sections "Characterization of the Deposition Rate Distribution Using 2D Experiments" and 5.1). In such a way, the deposition efficiency is implicitly accounted for in the simulations (at least at the first order).

In order to assess the capabilities and limitations of the proposed numerical model, simulations of a real industrial test case are performed, and the results are compared to experimental measurements of the footprint thickness. The selected test case is the thermal spray coating of a 3D aeronautical part containing three sharp teeth and involving a complex source trajectory with two different source velocities and orientations (see section "Industrial Coating Test Case on a 3D Object").

Experimental Procedure

In the present study, the chosen coating consists in the spraying of a NiAl alloy with [90 ± 45] µm grain size. The coatings were made with plasma gun connected to an ABB six-axis robot.

Section "Characterization of the Deposition Rate Distribution Using 2D Experiments" describes the experimental procedure to characterize the deposition rate profile using simple 2D (plane surface) test cases. Section "Industrial Coating Test Case on a 3D Object" presents the 3D aeronautic test case used to assess the numerical model in section "Model Assessment".

Characterization of the Deposition Rate Distribution Using 2D Experiments

The coating formation is driven by the rate of material deposition on the surface. The deposition rate distribution is an input of the proposed numerical model and needs to be characterized experimentally. Simple 2D coating experiments are (*a priori*) enough to characterize the deposition rate profile since the goal of the proposed numerical model is to deal with all the 3D aspects of more complex 3D coating process (3D surface geometries and trajectories).

The coating is applied to an Inconel 718 flat substrate (150 × 60 × 5 mm). Figure 1 illustrates the experimental device. The plasma gun has a normal orientation to the substrate with transverse cycles of forward and backward movements at speed between 200 and 700 mm/s. The number of cycles was adjusted in order to have a thickness between 400 and 800 μm.

The study of the macroscopic shape of the NiAl bead was carried out with an Alicona Infinitefocus G4 3D high-resolution optical microscope. The topographies were measured with × 10 and × 5 lenses and a vertical pitch of 100 nm and 410 nm. The average transverse thickness profile shown in Fig. 2 is obtained from the measurement of three profiles taken randomly over the entire bead. In section "Adjustment of the Deposition Rate Distribution Using 2D Coating Experiments", the experimental thickness profile on the 2D sample will be used to adjust the deposition rate distribution for subsequent 3D coating simulations.

Industrial Coating Test Case on a 3D Object

Figure 3 illustrates the experimental device. The substrate of the industrial case is a cylindrical like part with three seal teeth used in high-pressure compressor of civil aircraft engines. The thermal spray parameters are identical to
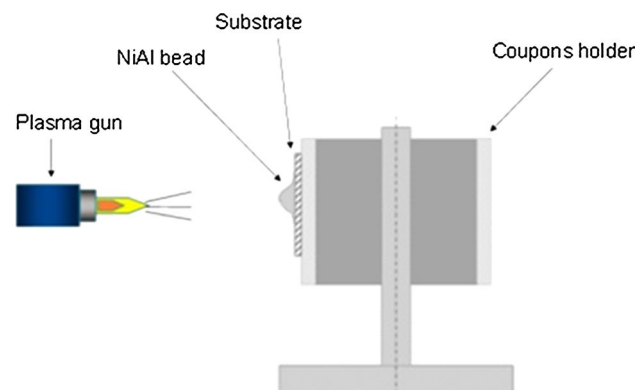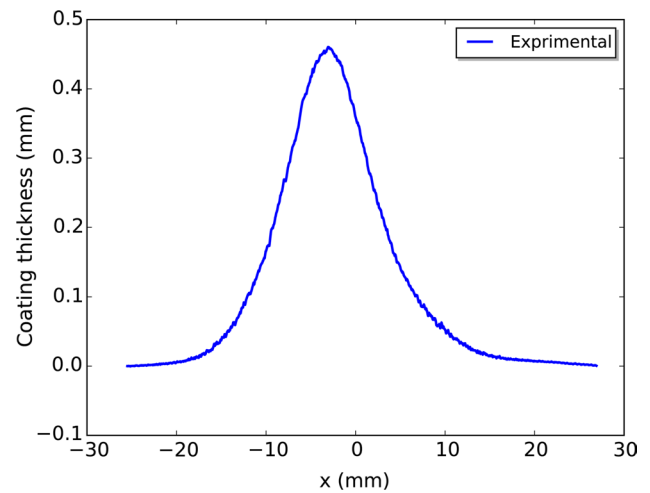

Fig. 2 Average coating thickness profile of the coating bead on a plane surface

those of the 2D test case used for the characterization of the deposition rate distribution in section "Characterization of the Deposition Rate Distribution Using 2D Experiments". During the process, the part rotates a 180 round per minutes while the plasma gun follows a complex trajectory with the following properties:

- The plasma gun motion is a sequence of forward and backward horizontal displacements above the part with a speed between 10 and 40 mm/s. The value of speed is different for forward and backward motions.
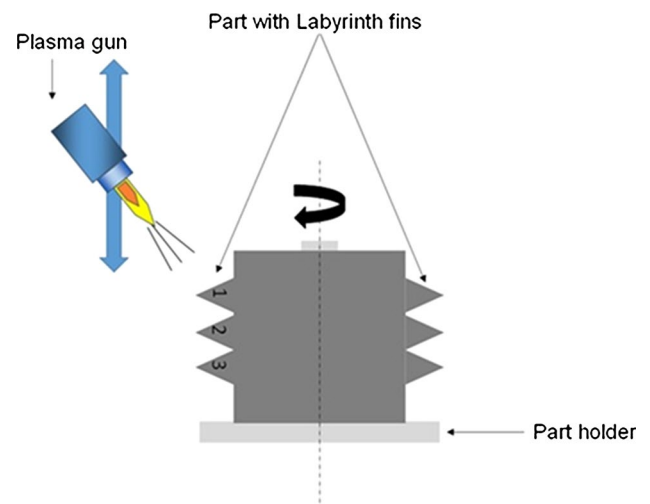- The angle between the plasma gun and the part axis is in the range between 20° and 35°. The value of angle is

Fig. 1 Scheme of the experimental device for the characterization of the deposition rate distribution

Fig. 3 Scheme of the experimental device for the industrial coating test case. The substrate is a 3D cylinder with seal teeth
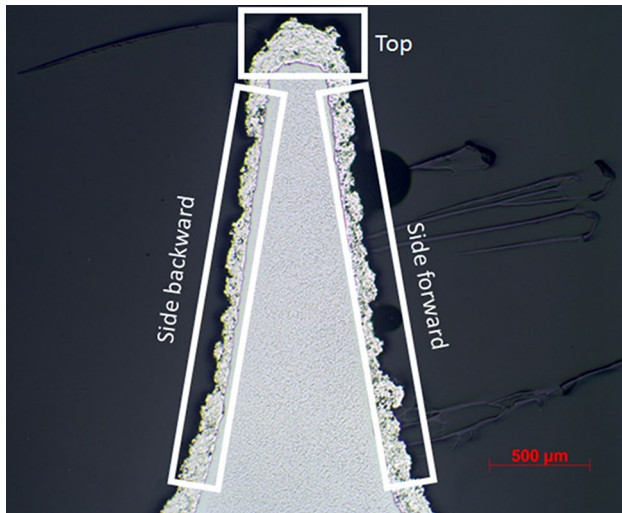
Fig. 4 Micrography cross section of a seal teeth after coating

Table 1 Average coating thickness in the tree zones of the seal teeth from micrography

Zone	Thickness, µm seal teeth 1	Thickness, µm seal teeth 2	Thickness, µm seal teeth 3
Top	206 ($\sigma = 21$)	216 ($\sigma = 14$)	221 ($\sigma = 28$)
Forward side	85 ($\sigma = 10$)	79 ($\sigma = 10$)	83 ($\sigma = 14$)
Backward side	75 ($\sigma = 8$)	70 ($\sigma = 11$)	70 ($\sigma = 11$)

different during forward and backward displacement of the source.

- The number of forward and backward cycles is adapted to reach a targeted thickness about 200 µm at the top of seal teeth.

To evaluate the coating thickness distribution on each seal teeth, an arbitrary area of interest is cut, polished and prepared to allow metallurgical cross-sectional observation and thickness measurements with an optical microscope Olympus PMG 3. The microstructure is characterized with ×200 magnitude. Figure 4 shows a cross section of the seal teeth and the zones where the thicknesses are evaluated. The seal teeth is divided into three zones: top, forward side and backward side. For each zone, the average value and the standard deviation the coating thickness is computed using the distance between the coating surface and the coating/substrate interface measured at different locations inside the zone.

The coating thickness for the three zones of each of the three seal teeth is given in Table 1. Given a standard deviation, there is no thickness difference in the same zone between each seal teeth. The larger thickness is observed at the top of the teeth, and the thickness on the forward side is larger than the

backward side due to the source angle and velocity which are different for forward and backward displacements.

Numerical Method

A numerical tool able to predict the shape and thickness of the coating footprint on a complex 3D object is proposed. To this aim, the level set method is used to compute the evolution of the object surface during the deposition process. A set of numerical methods is proposed to deal with the complex source trajectory and the shadowing effects, both strongly affecting the final footprint in the case of 3D objects coating. As explained in section "Proposed Numerical Methodology", a phenomenological approach is proposed to tackle the physical complexity related to the transport and interactions of the coating particles on the surface: the thermal spray source is not explicitly simulated but the overall mass transfer toward the surface is modeled by material deposition rate distribution adjusted using 2D coating measurements. The model is implemented into the finite element software Morfeo developed by Cenaero, and improvements in the numerical scheme are proposed to reduce the computational costs.

The Level Set Method

The level set method falls into the category of the front (surface) capturing approaches. The front (Γ) is not represented explicitly, instead it is described as the iso-zero surface of a higher dimensionality function: the level set function (ϕ). $\phi(\vec{x})$ is generally defined as the signed distance function to the front:

$$\phi(\vec{x}) = D(\vec{x}) = \min_{y \in \Gamma} |\vec{x} - \vec{y}| \operatorname{sgn}(\phi(\vec{x})) \tag{2}$$

The sign function is computed as:

$$\operatorname{sgn}(\phi(\vec{x})) = (\vec{x} - \vec{y}) \cdot \vec{n} \tag{3}$$

where $\vec{n}$ is the normal to the front at position $\vec{y}$.

The evolution of the front submitted to an imposed velocity field $\vec{v}$ is translated to an initial condition problem for the transport of ϕ (Ref 1):

$$\frac{\partial \phi}{\partial t} + \vec{v} \cdot \nabla \phi = 0 \tag{4}$$

If $\vec{v}$ is further decomposed in normal $\vec{n}$ and tangent $\vec{t}$ components relative to the front orientation

$$\vec{v} = v_n \vec{n} + v_t \vec{t} \tag{5}$$

and using the property of ϕ

$$\vec{n} = \frac{\nabla \phi}{|\nabla \phi|} \tag{6}$$

the level set transport equation becomes

$$\frac{\partial \phi}{\partial t} + v_n \frac{\nabla \phi}{|\nabla \phi|} \cdot \nabla \phi = 0 \tag{7}$$

This equation shows that the propagation of the front is driven by the component of the velocity normal to the front and will vary with respect to the angle between the imposed velocity and the surface normal.

Several algorithms have been proposed to solve the level set equation. In the present work, the level set transport problem is solved on an unstructured mesh (the so-called support mesh) using the "positive coefficient scheme" described in (Ref 1) coupled with an explicit second-order Runge-Kutta time integrator. As explained in (Ref 16), such a scheme does not need specific boundary conditions.

The narrow band technic is used to reduce the computational costs (Ref 1). The computational domain for the transport problem is restricted to a narrow band surrounding the current front. The width of the narrow band can be defined by the user and is further extended locally in the direction of the imposed velocity by an amount equal to the expected displacement (MaxDispl$(\vec{y}) = v_n(\vec{y}) * dt$ where dt is the time step). The narrow band evolves with the front during the transport process and the distance and velocity fields need to be recomputed for each time step in the new narrow band.

Numerical Scheme for the Coating of 3D Objects

In the present work, the level set method is used to track the evolution of the coating footprint during the coating process using a time-dependent iterative numerical scheme described in section "Description of the Time-Dependent Numerical Scheme". The source trajectory is discretized in time with a given time step dt, and the coating process is modeled as a sequence of spot-wise depositions. Consequently, dt must be small enough in order to simulate a continuous footprint while the computational costs are inversely proportional to dt.

Input Data

The input data requested for the coating simulation are divided into two groups: coating process parameters and numerical parameters.

The process parameters to be provided are

- The initial surface of the 3D object is provided as a triangle surface mesh and used to define the initial front Γ for the level set computations.
- The source trajectory and orientation is provided as a 1D polyline as explained in section "Numerical Model for the Source Trajectory and Orientation".

- The velocity of the source along the trajectory (v_s) is provided as a scalar value.
- The deposition rate distribution is provided as a 2D analytical function as described in section "Numerical Model for the Deposition Rate Distribution".

The numerical parameters to be provided are

- The support mesh surrounding the initial front provided as a simplex 3D mesh (tetrahedral elements). The spatial extension of the support mesh must be large enough to capture the front/footprint evolution during the process.
- The time step for the numerical integration (dt) is given as a scalar value.

Description of the Time-Dependent Numerical Scheme

The coating simulation is based on the following iterative procedure:

1. The imposed velocity field $\vec{v}(\vec{x})$ is computed based on the current source position $(\vec{p_s})$, direction $(\vec{d_s})$ and deposition rate distribution (Q). The velocity field $\vec{v}$ is first computed at each vertex of the current front/surface and the component normal to the surface v_n is evaluated using (Eq 5). v_n is set to zero in regions where $\vec{n} \cdot \vec{d_s} \leq 0$ to avoid deposition on backward facing surfaces. Shadowing effects also impose zero velocity in some regions as explained in section "Numerical Model for the Shadowing Effects". The narrow band region of the support mesh is defined based on the surface velocity values as described in section "Narrow Band Scheme Improvement". The velocity field is then extended from the surface into the narrow band region though a nearest neighbor approximation.

2. The level set function $\phi(\vec{x})$ is computed for each vertex of the narrow band using the signed distance function (Eq 2). The minimal distance is computed using triangle-to-point distance algorithms. The computation of the minimal distance to the whole front requires to loop on all the triangles defining the surface. In order to reduce the computational costs, the loop is restricted to a subset of triangles close to $\vec{x}$ detected using a search tree algorithm.

3. The level set transport equation (Eq 7) is solved into the narrow band leading to an updated level set function $\phi(\vec{x})$.

4. The new front/surface mesh is computed using a mesh cutting algorithm at the iso-0 of the level set function.

5. The source is then displaced following the prescribed trajectory and time step leading to a new velocity field

and an updated front. These operations are repeated until the end of the source trajectory.

Numerical Model for the Source Trajectory and Orientation

To obtain a uniform footprint on a 3D object, the source and/or the object are moved during the coating process. Therefore, the spatial distribution of the imposed velocity field $\vec{v}(\vec{x})$ will evolve during the process. In the present method, the object is considered as static and the source travels around the object following a user-defined trajectory at an imposed velocity v_s.

The source trajectory is defined as a 1D polyline in the 3D space. The evolution of the source direction is defined using local direction vectors associated with each point of the trajectory.

At a given time iteration during the coating simulation, the current source position is computed using linear interpolation between the two closest trajectory points, while the current source direction is computed using a quaternion "slerp" interpolation scheme (Ref 17).

Numerical Model for the Deposition Rate Distribution

The definition of the velocity field amplitude $\left|\vec{v}(\vec{x})\right|$ is a critical part of the model since it directly affects the thickness of the deposited layer. In reality, $\left|\vec{v}(\vec{x})\right|$ must reflect the volumetric rate of deposition of the coating particles on the surface. This quantity involves a lot of complex physical and chemical phenomena related to the interactions between the heating particles and the plasma (thermal transfer affecting the particle melting, momentum transfer driving the particles trajectories and velocities…). In addition, it is also necessary to consider the complex interactions between the particles and the target surface (splattering, deposition angle, surface roughness, materials, temperature…). A numerical model resolving all these aspects would be computationally prohibitive.

To reach numerical prediction of the coating footprint within affordable computational costs, a phenomenological approach is proposed here: $\left|\vec{v}(\vec{x})\right|$ is defined using an analytical distribution function describing the volumetric deposition rate in a plane normal to the source direction: $Q(x_s, y_s, z_s; P)$, where $(\vec{x_s}, \vec{y_s}, \vec{z_s})$ is the coordinates system of the source, with $\vec{z_s}$ is aligned with the current source direction and P is a set of free parameters.

The free parameters P are adjusted to fit with the experimental footprint thickness distribution obtained from simple plane surface coating as described in section "Characterization of the Deposition Rate Distribution Using 2D Experiments". In such a way, $Q(x_s, y_s, z_s)$ implicitly includes the major physicochemical phenomena involved in the deposition process (at least those accounted for in the simple tests case).

Numerical Model for the Shadowing Effects

In the case of complex 3D geometries, some parts of the surface may hide other parts leading to shadowed regions where no deposition occurs. The shadowing effect has a strong impact on the deposition footprint and need to be considered during the simulations.

The shadowed region depends on the instantaneous position and the orientation of the object with respect to the spraying source. A ray-tracing algorithm has been developed to detect shadowed regions during the deposition process. For each vertex of the current surface, a line segment is defined from the vertex to its projected position on the plane normal to the current source position. All the triangles of the potentially shadowing surfaces (the surface itself and/or masks used to impose shadows in specific regions) are then tested with a segment/triangle intersection algorithm (Ref 18). If a triangle intersects a segment, the corresponding vertex is considered as shadowed and the imposed velocity at this vertex is set to zero.

In order to reduce the potentially prohibitive number of [segment, triangle] pairs to be evaluated, a cell structure is proposed. The surface/mask mesh is first projected on the plane normal to the current source direction. This plane is then divided in square cells with size of the order of the smallest triangle dimension. For each triangle, the reduced list of potentially shadowed vertices is constructed to include all the vertices belonging to the cells spanned by the triangle.

Narrow Band Scheme Improvement

Due to the limited extension of the source and/or nonmatching local surface with respect to source direction and/or shadowing effects, only a subset of the current surface is submitted to nonzero deposition rate (or level set velocity).

In order to further reduce the computational cost, the narrow band is restricted to this surface subset which is automatically updated throughout the simulation. Consequently, all the level set operations (cutting the iso-0 surface, distance computation, shadowing and level set transport) are performed on a reduced domain.

Model Assessment

Adjustment of the Deposition Rate Distribution Using 2D Coating Experiments

The deposition rate distribution is approximated by a 2D Gaussian function in a plane normal to the current source direction:

$$Q(x_s, y_s, z_s) = G_{2d}(x_s, y_s, z_s) = \mathrm{IN}/(\pi r^2)e^{-N(x_s^2 + y_s^2)/r^2} \quad (8)$$

where x and y are coordinates in the normal plane, I is the deposition rate intensity (mm³/s), r is the distribution radius (mm) and N is a parameter controlling the distribution variance (set to 4. in the following leading to $r = \mathrm{sqrt}(N*2)*\sigma = 2.83*\sigma$, where σ is the standard deviation of the 2D Gaussian function).

The parameters I and r are adjusted to fit the experimental measurement of footprint thickness obtained with the training test cases presented in section "Characterization of the Deposition Rate Distribution Using 2D Experiments". The adjustment procedure is based on the numerical integration of $G_{2d}(x_s, y_s, z_s)$ along the experimental source trajectory coupled with a "Nelder–Mead" optimization algorithm.

The obtained parameters values are $I = 145.17$ mm³/s and $r = 15.11$ mm. The fitted Gaussian profile is close to the experimental measurements as shown in Fig. 5. However, the experimental profile is asymmetric which limits the quality of the adjustment with a symmetric Gaussian distribution (especially for $x > 0$ as illustrated in Fig. 5). This footprint non-fully-symmetry is probably due to the injection of particles in the plasma torch (Ref 19).
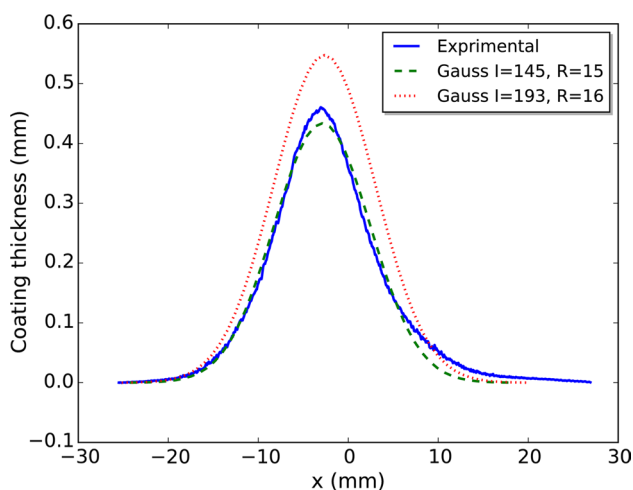
The adjusted source intensity (145.17 mm³/s) is lower than the measured rate of material consumption (193.3 mm³/s $\pm$ 10%). This is probably due to the asymmetry issue explained above and the deposition efficiency effects described in section "Proposed Numerical Methodology". Another cause may be related to the experiment itself. Indeed, in normal spraying, the lighter/smaller particles tend to follow the plasma streaming line, which goes away from the target surface leading to a lower deposition rate compared to the material consumption rate (Ref 20). A second deposition rate distribution is proposed to better reproduce the material consumption. In this second adjustment, I is imposed to 193.3 mm³/s and only r is adjusted to the value of 16.43 mm leading to the second curve in Fig. 5. As expected, increasing the deposition rate intensity leads to an increase in the final coating thickness.

Coating Simulation Setup

Geometry and Meshing

The seal teeth part geometry is described in section "Industrial Coating Test Case on a 3D Object". Since this geometry has a symmetry of revolution, the simulation domain is restricted to a small angular sector (pi/384) as shown in Fig. 6. This allows to reduce the computational costs without affecting the quality of the numerical predictions.

The meshing operations are performed using the free package gmsh v3.0. The object surface is meshed using simplex (triangle) elements. This surface mesh is the initial front in level sets computations.

The unstructured support mesh for the level set computations is shown in Fig. 7. A fine mesh is used in the region of interest (i.e., around the three seal teeth), while a coarser mesh is used far from the initial surface in order to reduce
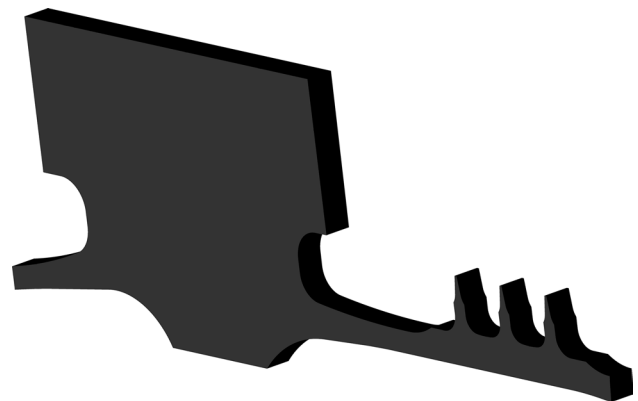

Fig. 5 Comparison of the experimental footprint profile (solid) and the fitted Gaussian profiles (dashed: adjusted $I = 145.16$ and $r = 15.11$, dotted: imposed $I = 193.3$ mm³/s and adjusted $r = 16.43$)

Fig. 6 Geometry of the seal teeth parts used in the simulations. The geometry is restricted to an angular sector of pi/384

Fig. 7 Support mesh for the level set computations

the computational costs. The mesh size in the region of interest is set to 50 μm.

Setup of the Thermal Spray Source Model

As explained in section "Industrial Coating Test Case on a 3D Object", the coating procedure involves a fast rotation of the seal teeth part coupled with a linear cyclic motion of the spraying source. Since the current numerical scheme does not support the motion of the object, these two motions are regrouped into a single helicoidal motion of the source around the static parts as shown in Fig. 8. The whole set of forward and backward cycles is simulated within a single kinematic. A small offset is imposed between the successive cycles to avoid the exact superposition of the source trajectory and ensure a uniform deposition on the target surface. In practice, since only a small sector of the seal teeth part is simulated, the helicoidal trajectory is also truncated to a small angular sector to reduce the computational costs.

The different source direction and velocity for the forward and backward source displacements are considered. A snapshot of the spraying source directions with respect to the support mesh is shown in Fig. 9.

Finally, the Gaussian deposition rate distribution as defined in section "Numerical Model for the Deposition Rate Distribution" is imposed. In order to further reduce the computational costs through the current deposition region mechanism (see section "Numerical Scheme for the Coating of 3D Objects"), the deposition rate distribution is truncated at a distance r_cut using the following analytical function:
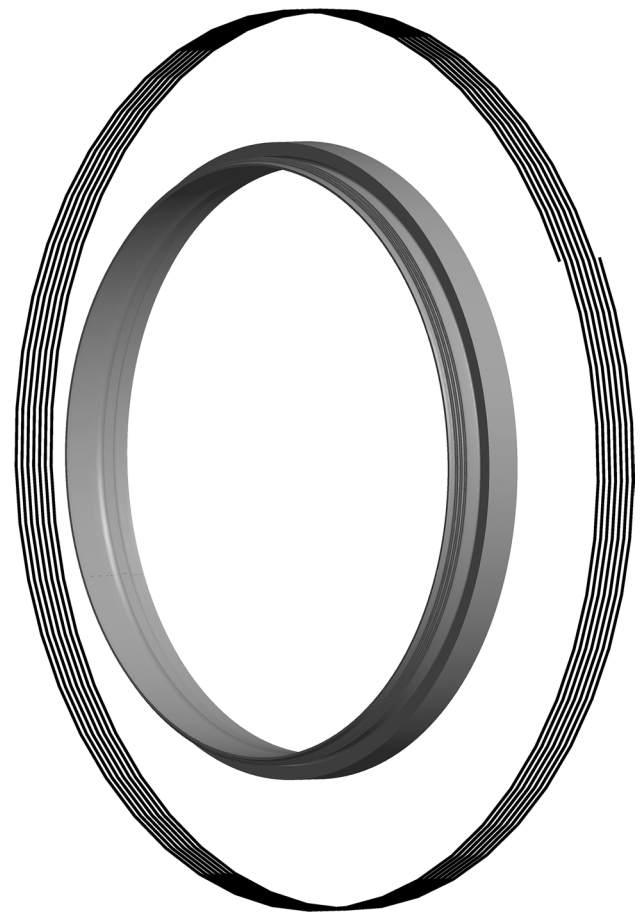

Fig. 8 Full helicoidal trajectory of the source around the seal teeth parts corresponding to a single forward motion

$$S(x, y) = G(x, y) * \mathrm{Tr}(x, y)$$

$$= \mathrm{IN}/(\pi r^2) e^{-N(x^2+y^2)/r^2} * \left(1 - \tanh\left(\left(\sqrt{(x^2+y^2)} - r_{\mathrm{cut}}\right)/1e-6\right)\right)/2 \tag{9}$$
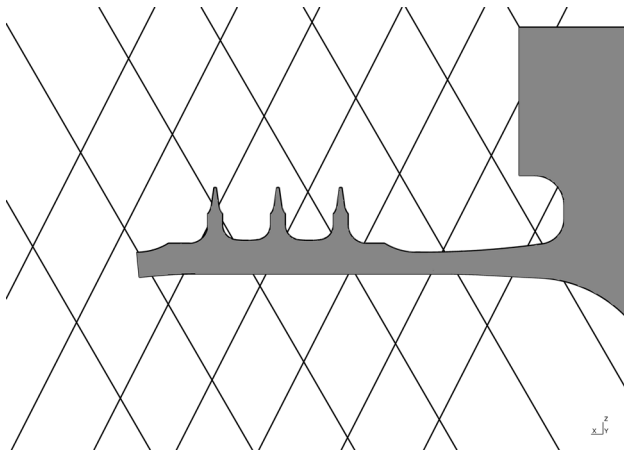
Fig. 9 Visualization of the source directions for a single forward and backward source cycle. Each line corresponds to the source direction imposed at a vertex of the source trajectory polyline
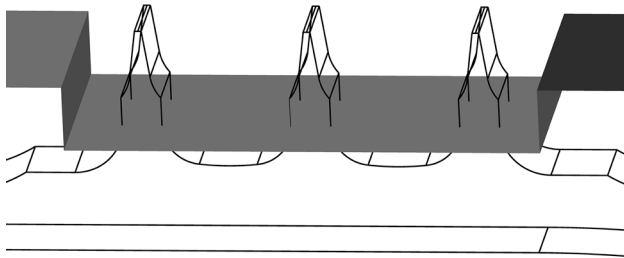

Fig. 10 Snapshot of the masking surface on the seal teeth part sector

In practice, r_cut is set equal to the radius of the Gaussian deposition rate distribution ($r = 2.83\sigma$). Since $r = \text{sqrt}(2\,N)\sigma = 2.83\sigma$, the volume loss due to the truncation is negligible (<1%).

Masking Surfaces

Masking surfaces are used in the experimental trials to avoid deposition in selected regions. The masks are also considered in the simulations as shown in Fig. 10. The masks avoid the deposition at the bottom of the three seal teeth through the use of the shadowing method described in section "Numerical Model for the Shadowing Effects".

Time Integration

The time step value has a strong impact on the simulated footprint. Using large time step will lead to an unphysical spot-wise footprint since successive iterations will create disconnected "spot" footprint. On the other hand, small time steps will increase the computation duration as the number of iterations will increase. A good tradeoff is to impose a

time step such that the distance between the centers of two successive spots is one third of the Gaussian radius. In the present test case, this leads to time steps of 1e − 3s.

Analysis of the Simulation Results

Description of the Numerical Predictions

The simulations are performed with a deposition rate intensity $I = 145$ mm^3/s and radius $r = 15$ mm and a uniform support mesh size of 50 μm and a time step of 1e − 3s. The final footprint is post-treated to obtain the transverse section map of coating thickness shown in Fig. 11. The following observations are made:

- The footprint on the three teeth is very similar with a maximum thickness difference lower than 1 μm observed at the top. This is consistent with the experimental observations in section "Industrial Coating Test Case on a 3D Object".
- The largest thickness is observed at the top of the peaks (144.4 μm). The thickness on the forward side (52.6 μm) is larger than on the faces in front of the backward side (46.9 μm). The observed thickness distribution is due to the complex source trajectory, orientation and velocity combined with the shape of the target surface leading to variation of the local deposition angle and rate. The difference of thickness between the forward and backward faces is due to the different source orientations and velocities during forward and backward source motion. At the top of the peaks, deposition occurs during both forward and the backward source motion leading to a thicker footprint. Note that the predicted coating thickness at the top of the teeth is roughly equivalent to the value of the source intensity used for the computation. This is purely fortuitous as other source trajectories, number of cycles and/or source velocity will change the thickness value as explained in the parameter sensitivity analysis described in the next section. These observations are also consistent with the experimental measurements described in section "Industrial Coating Test Case on a 3D Object".
- In the curved region below the planar faces, the thicknesses increase since the surface normal is closer to the source orientation for both backward and forward directions (see Fig. 9).
- At the bottom of the peaks, no deposition occurs due to the imposed masking surfaces (see Fig. 10). This indicates that the shadowing method is working properly.

These observations indicate that the proposed model can predict the combined effects of the source parameters (trajectory, orientation, velocity and intensity) and the geometry

Fig. 11 Snapshot of the numerical footprint on the seal teeth in the forward side (a) and backward side (b)
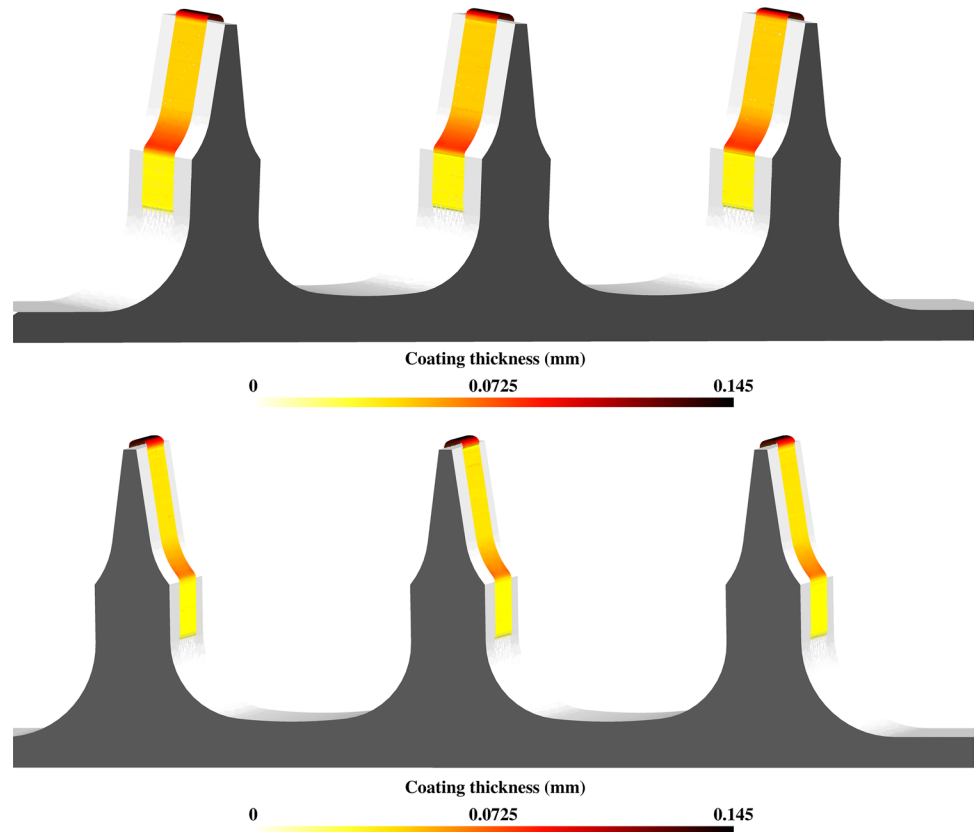
of the target 3D surface on the final footprint. A deeper comparison with the experimental measurements is provided in section "Assessment of the Model Through Comparison with Experimental Results". In the following section, a sensitivity analysis is performed to estimate the influence of both the numerical and the process parameter on the footprint predictions.

Parameter Sensitivity Analysis

A parameter sensitivity analysis has been performed to study the impact of numerical and process parameters on the predicted coating thickness:

- Numerical resolution: The numerical results are converged with the selected mesh size of 50 μm and time step of $1e-3$s. Indeed, simulation with space and time resolutions increased by a factor 2 leads to a maximal thickness variation below 1%.
- With a truncation radius equal to the source radius ($r\_cut = r$; see Eq 9), the coating thickness is uniformly reduced by 1 μm while the computation duration is reduced by a factor of 3 which means that the truncation could be applied safely without degrading the numerical results. However, a significant sensitivity is observed for truncation radius smaller than r.

- The source trajectory and velocity have a significant impact on the predicted coating thickness. As expected through simple volume conservation criteria, the predicted coating thickness is proportional to the number of forward/backward cycles, inversely proportional to the source velocity and proportional to the sinus of the local beam incident angle. As an example, if the source orientation and velocity of the forward source motion are also used for the backward motion, the same thickness values are predicted on both the forward and backward faces of the teeth.
- The sensitivity to the source radius (r in Eq 8) is low. The same coating thickness is obtained with radius increased to 20 mm or reduced to 7.5 mm while keeping the same source intensity (I in Eq 8). It is due to the imposed trajectory in which the distance between two successive forward (or backward) cycles is one order of magnitude smaller than the source radius.
- On the other hand, the deposition rate intensity (I in Eq 8) is a sensitive parameter. As expected, the predicted thicknesses are directly proportional to the deposition rate intensity. This is shown in Fig. 12 in which the footprint obtained with two different set of source parameters are compared. The ratio of coating thickness at the top of the teeth is equivalent to the ratio of imposed source intensity ($145/193 = 0.75$).

Fig. 12 Comparison of the numerical footprints obtained with source parameters [$I = 145$, $r = 15$] (the thinner footprint) and [$I = 193$, $r = 16$] (the larger footprint)
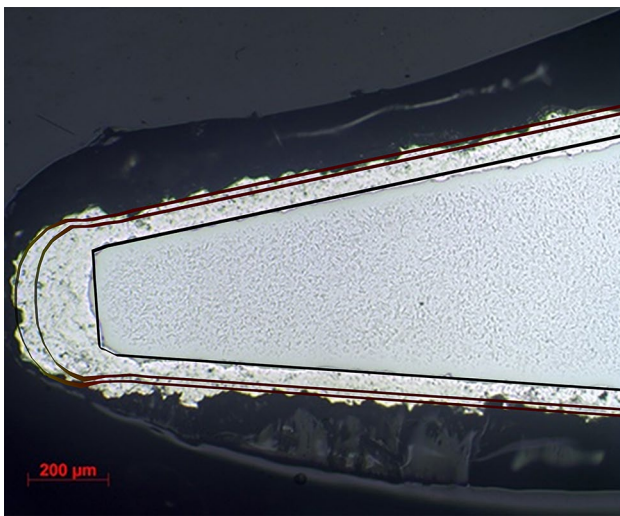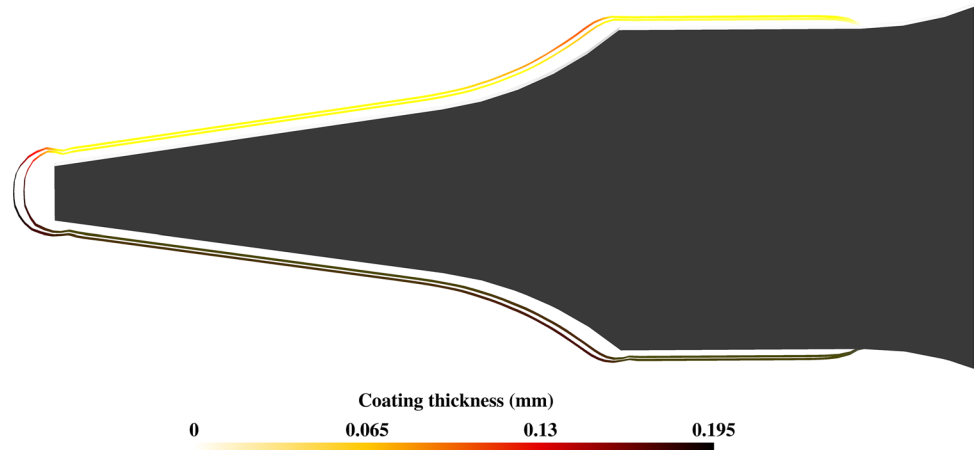

Fig. 13 Comparison of the experimental (micrograph) and numerical (superimposed lines) footprints obtained for the aeronautic test case. The two numerical footprints are obtained with different values of the deposition rate intensity: 145 mm³/s for the thinner footprint and $I = 193$ mm³/s for the larger footprint

As a summary, the numerical parameters have few impacts on the results and the simulation shows that the main process parameters affecting the footprint are the source trajectory and the deposition rate intensity.

Assessment of the Model Through Comparison with Experimental Results

A preliminary qualitative assessment of the numerical model is done through the comparison of numerical and experimental footprint images shown in Fig. 13. The experimental footprint shows high roughness arising from the particle deposition process which is not reproduced by the present continuous model. However, for both deposition rate values ($I = 193$ and 145 mm³/s), the overall shape of the predicted footprints is close to the experimental footprint. The footprint thickness obtained with $I = 193$ mm³/s is larger and closer to the experiments.

A quantitative assessment is performed using local coating thickness and thickness ratio values given in Table 2. The experimental and numerical values are evaluated at three different locations: the top of the tooth (T) and the centers of the forward and backward sides of the teeth (F and B).

The numerical thicknesses obtained with a source intensity $I = 145$ mm³/s are about 35% lower than the experimental measurements for all three locations. With a source intensity increased to 195 mm³/s, the difference is reduced to 10%, within the experimental standard deviation (surface roughness). Such results tend to indicate that the numerical model can be used to predict the magnitude of the coating

Table 2 Comparison of numerical and experimental coating thickness at three different locations (T top of the teeth, F teeth face in front of the source forward motion direction, B teeth face in front of the source backward motion direction). The two last columns are the thickness ratios between the locations T/F and B/F

Location	Coating thickness, μm			Thickness ratio	
	T	F	B	T/F	B/F
Experiments	214.3 (σ=21.)	82.3 (σ=11.)	71.7 (σ=10.)	2.60	0.87
Numeric $I = 145$ mm³/s	144.4	52.6	46.9	2.74	0.89
Numeric $I = 193$ mm³/s	193.8	70.2	62.4	2.76	0.89

thickness. However, the accuracy of the thickness predictions strongly depends on the adjustment of the deposition rate distribution parameters (in present test case, the deposition rate intensity).

The two last columns of Table 2 give the ratios of coating thicknesses between T/F and B/F. These ratios allow to quantify the (non-)uniformity of the footprint thickness on the 3D object, which is a very useful information to characterize the final coating properties and performances. Contrary to the thickness amplitudes, the thickness ratios are not significantly affected by the value of the deposition rate intensity. Instead, the thickness ratios depend on the motion of the source: the B/F ratio is different from one due to the different source orientations and velocities during forward and backward source motion, while the T/F ratio is larger than one since deposition at the top of the teeth occurs for both motion directions. For both ratios, the numerical predictions are close to the experimental measurements with a maximum difference of the order of 5% for the T/F ratio. This illustrates the capability of the model to correctly predict the impact of the source motion on the footprint uniformity on a complex 3D object.

As expected, the source motion seems to be the main parameter affecting the final footprint uniformity while the coating thickness amplitude is mainly driven by the material deposition rate intensity.

Conclusions

A numerical method to predict the footprint of thermal spray coating process on 3D object has been presented through this paper. It is based on the level set method to track the evolution of the footprint considering the local orientation of the surface with respect to the orientation of the source. It is coupled with numerical tools to deal with the specific feature of 3D objects coating regarding the complex source motion and the shadowing effects. The physics of the deposition process itself is described using a phenomenological approach through an analytical function representing the distribution of the deposition rate in the plane normal to the current source orientation. The parameters of the distribution are adjusted to fit with experimental measurements of the footprint thicknesses profile obtained from simple coating test cases normal to a planar surface.

The proposed numerical tool is assessed through an application on thermal spray coating of a real aeronautic component. The numerical tool is able to predict the shape of the footprint taking into account the complex spraying source trajectory and the shadowing effects. The distribution of coating thickness on the object surface is well reproduced which indicates that the model can be used to estimate the impact of process parameters on the uniformity of the final coating. The model also allows to predict the order of magnitude of the footprint thickness. However, the predicted thickness values are sensitive to the value of the deposition rate intensity which needs to be adjusted carefully if quantitative predictions are expected.

The model is implemented into the finite element software Morfeo developed by Cenaero which allows for further coupling with the Morfeo thermo-mechanical solver to predict the mechanical properties of the final coating layer and/or the thermal history of the system during the coating process. Moreover, the proposed coating model can be further improved to account for the deposition efficiency as a function of the surface and particles thermo-mechanical properties (Ref 15).

References

1. R.C. Tucker, *ASM Handbook Volume 5A Thermal Spray Technology*, ASM International, New York, 2013
2. B. Walser, The Importance of Thermal Spray for Current and Future Applications in Key Industries, *Spraytime*, 2004, **10**(4), p 1-7
3. P. Fauchais, J.V.R. Heberlein, and M. Boulos, *Thermal Spray Fundamentals from Powder to Part*, Springer, US, 2014
4. S. Cirolini, J.H. Harding, and G. Jacucci, Computer Simulation of Plasma-Sprayed Coatings I, *Coat. Depos. Model Surf. Coat. Technol.*, 1991, **48**(2), p 137-145
5. F.-I. Trifa, G. Montavon, and C. Coddet, On the Relationships Between the Geometric Processing Parameters of APS and the Al_2O_3-TiO_2 Deposit Shapes, *Surf. Coat. Technol.*, 2005, **195**(1), p 54-69
6. X. Chen and H.-P. Li, Three-Dimensional Flow and Heat Transfer in Thermal Plasma Systems, *Surf. Coat. Technol.*, 2003, **171**(1-3), p 124-133
7. T.H. Ko and H.K. Chen, Three-Dimensional Isothermal Solid–Gas Flow and Deposition Process, *Surf. Coat. Technol.*, 2005, **200**(7), p 2152-2164
8. D.T. Gawne, B. Liu, Y. Bao, and T. Zhang, Modelling of Plasma–Particle Two-Phase Flow Using Statistical Techniques, *Surf. Coat. Technol.*, 2005, **191**(2-3), p 242-254
9. S. Gu and S. Kamnis, Numerical Modelling of In-Flight Particle Dynamics of Non-spherical Powder, *Surf. Coat. Technol.*, 2009, **203**(22), p 3485-3490
10. K. Remesh, H.W. Ng, and S. Yu, Influence of Process Parameters on the Deposition Footprint in Plasma-Spray Coating, *J. Therm. Spray Technol.*, 2003, **12**(3), p 377-392
11. S. Kotowski, M. Sieniawski, and M. Goral, Modelling and Simulation of Plasma Spraying Process with a Use of Jets&Poudres Program, *J. Achiev. Mater. Manuf. Eng.*, 2012, **55**(2), p 547-550
12. J.G. Goedjen, R.A. Miller, W.J. Brindley, and G.W. Leissler, *A Simulation Technique for Predicting Thickness of Thermal Spray Coatings, NASA-TM-106939*, NASA Lewis Research Center, Cleveland, 1995
13. M.M. Fasching, F.B. Prinz, and L.E. Weiss, Planning Robotic Trajectories for Thermal Spray Shape Deposition, *J. Therm. Spray Technol.*, 1993, **2**(1), p 45-50

14. D.A. Stepanenko, Modeling of Spraying with Time-Dependant Material Feed Rate, *Appl. Math. Model.*, 2007, **31**(11), p 2564-2576

15. F. Fanicchia and D. Axinte, Transient Three-Dimensional Geometrical/Thermal Modelling of Thermal Spray: Normal-Impinging Jet and Single Straight Deposits, *Int. J. Heat Mass Transf.*, 2018, **122**, p 1327-1342

16. J. Sethian, *Level Set Methods and Fast Marching Methods. Evolving Interfaces in Computational Geometry, Fluid Mechanics, Computer Vision, and Materials Science*, 2nd ed., Cambridge University Press, Cambridge, 1999

17. K. Shoemake, Animating Rotation with Quaternion Curves, *ACM SIGGRAPH Comput. Gr.*, 1985, **19**(3), p 245-254

18. J.J. Jimenéz, R.J. Segura, and F.R. Feito, A Robust Segment/Triangle Intersection Algorithm for Interference Tests, *Comput. Geom.*, 2010, **43**(5), p 474-492

19. H.-B. Xiong, L.-L. Zheng, S. Sampath, R.L. Williamson, and J.R. Fincke, Three-Dimensional Simulation of Plasma Spray: Effects of Carrier Gas Flow and Particle Injection on Plasma Jet and Entrained Particle Behavior, *Int. J. Heat Mass Transf.*, 2004, **47**(24), p 5189-5200

20. M. Jadidi, S. Moghtadernejad, and A. Dolatabadi, A Comprehensive Review on Fluid Dynamics and Transport of Suspension/Liquid Droplets and Particles in High-Velocity Oxygen-Fuels (HVOF) Thermal Spray, *Coating*, 2015, **5**(4), p 576-645